Efficient Analysis of Highly Resonant Transmitarray Element For Sub-THz 6G Communications

Daniel R. Prado, Xuekang Liu, *Member, IEEE,* Rosa Letizia, *Senior Member, IEEE,* Claudio Paoloni, *Senior Member, IEEE,* and Lei Wang, *Senior Member, IEEE*

***Abstract*—An efficient analysis technique for a transmitarray (TA) unit cell based on a method of moments (MoM) in the spectral domain assuming local periodicity is proposed. The MoM employs basis functions consisting of Chebyshev polynomials weighed by a function that accounts for edge singularities. The analysis technique is applied to a unit cell consisting of two sets of five parallel dipoles that are shifted one with respect to the other to create a Huygens resonance that maximizes transmission of the impinging plane wave. Comparisons with circuit models show that the proposed technique achieves better accuracy while providing significant computational gains compared with commercial general purpose software. Finally, a unit cell is optimized to work in the W-band with the aim of employing it to the design of TAs for ultra-capacity fixed wireless links.**

***Index Terms*—Transmitarray, unit cell, transmission coefficients, method of moments (MoM), periodic structure**

I. Introduction

INCREASING demand for higher data rates and lower latency coupled with the saturation of the sub-6 GHz spectrum has led to the use of millimetre-wave spectrum for 5G and future 6G new radio networks [1], [2]. In particular, the International Telecommunication Union (ITU) has established, among others, the range 102 GHz–109.5 GHz in the W-band of particular interest for the development of telecommunication services [3]. These sub-THz [4] frequency bands offer the possibility of exploiting larger frequency bands of unused spectrum to provide backhaul and fronthaul to enable future 6G applications such as enhanced mobile broadband, massive machine-type communications and ultra-reliable and low-latency communications [3].

One limiting aspect of employing sub-THz bands is the limited transmission power of transceivers [5] as well as the high propagation losses of free space [6]. This leads to the need of high gain directional antennas. Among the proposed antenna technologies to overcome these challenges are transmitarrays (TA) [7] due to their low profile and low manufacturing costs while providing high gain performance and the possibility to easily control the transmitted electromagnetic waves [8]. Some TAs have already been proposed that work at sub-THz frequencies [9]–[12]. A common approach for the design of these arrays is to employ general purpose electromagnetic software with periodic boundaries for the analysis of the unit cell. However, there is a trade-off between flexibility and computational cost, leading to large design and optimization time. Another approach is the development of a numerical technique for the analysis of unit cells. The method of moments (MoM) [13] remains a popular choice that has been used for many years in reflectarray antenna design [14]–[17]. However, the design and optimization of TAs has not benefited so far from the efficiency that this approach provides.

In this work, a MoM in the spectral domain assuming local periodicity is proposed for the electromagnetic analysis of TA unit cells, allowing to efficiently obtain the full matrix of transmission coefficients. The MoM employs Chebyshev polynomials that include edge singularities to model the electric current in the metallizations. Then, the technique is applied to the analysis of a TA unit cell consisting of two shifted sets of five resonant dipoles [18]. Compared with simulations based on a circuit model, the proposed technique offers more accuracy while achieving substantial computational gains when compared to general purpose commercial software. Finally, the MoM is employed to find optimal parameters of a unit cell at W-band with the aim of employing it for the design of TAs for ultra-capacity fixed wireless links. It is worth mentioning that, as a trade-off between generality and computational efficiency, the technique described in this work is not able to account for vias, which are common in receiver-transmitter structures of transmitarray unit cells [19], [20]. However, other types of metallizations could be considered with a proper choice of basis functions [13].

II. Analysis of Ultrathin Huygens Unit Cell

A. Unit Cell Description

Fig. 1 shows the unit cell. It is based on that of [18] where the metallizations are dipoles defined by their width w, length $l_{q,i}$ and centre coordinates $(x_{c,q,i}, y_{c,q,i})$, where $q = 1, 2$ indicates the metallization interface, and $i = 1, \ldots, 5$ is the metallization number at each interface. There are two sets of five parallel dipoles. Each set is placed on each side of the substrate, and they are shifted with respect to each other. The substrate can be characterised by a complex permittivity $\varepsilon = \varepsilon_r \varepsilon_0 (1 - j \tan\delta)$ that accounts for substrate losses.

The working mechanism of the unit cell is to generate a Huygens resonance that enables a highly efficient transmission with electrically very thin layers [21], [22]. This is achieved by generating a pair of in-phase orthogonally induced electric

This work has been supported by the EPSRC grant EP/Y003144/2, and by Innovate UK SBRI: Future Telecommunications Challenge No. 10102343. *(Corresponding author: Daniel R. Prado.)*

The authors are with the School of Engineering, Lancaster University, U.K. (e-mail: d.rodriguezprado@lancaster.ac.uk).

Digital Object Identifier XX.XXXX/LAWP.XXXX.XXXXXXX

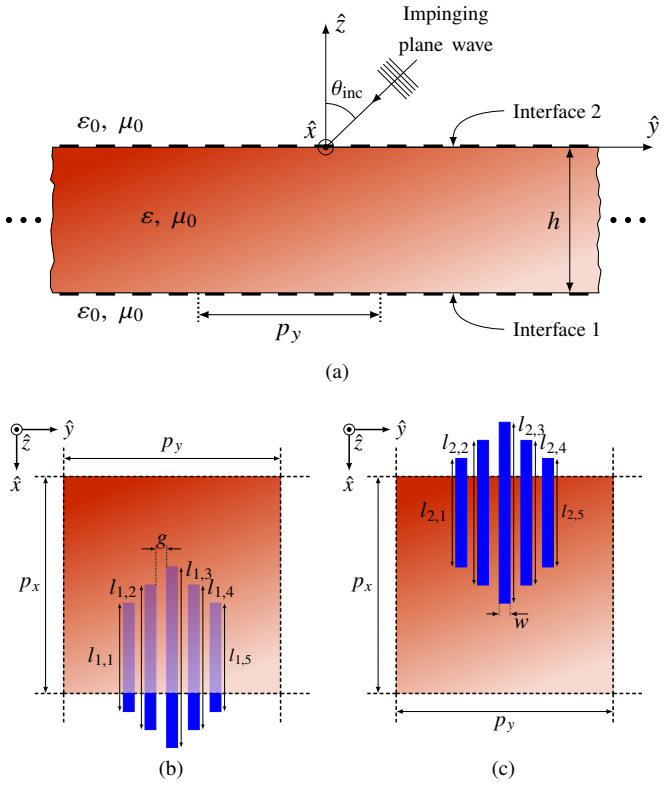

Fig. 1. (a) Lateral view, and top view of the (b) bottom layer and (c) top layer of the ultrathin transmitarray unit cell. The dipoles are printed on both sides of a single substrate slab and are defined by their length, width and coordinates of their centre, which are denoted as $(x_{c,q,i}, y_{c,q,i})$, $q = 1, 2$ (interface), $i = 1, \ldots, 5$ (dipole number).

and magnetic currents. In the present case, the resonance is achieved by tuning both the overlap between the two sets of dipoles as well as the length of the dipoles. The operating physical mechanism for the unit cell shown in Fig. 1 has been studied in [18] by means of a circuit model plus full-wave simulations of the unit cell.

B. Electromagnetic Characterization of the Unit Cell

The electromagnetic characterization of the unit cell requires the computation of a 2×2 matrix of complex transmission coefficients $\overline{T}$. This matrix relates, in Cartesian coordinates, the tangential incident ($\vec{E}^{\text{inc}}$) and transmitted ($\vec{E}^{\text{tra}}$) fields, which are defined in the top and bottom interfaces of the unit cell, respectively, as:

$$\begin{pmatrix} E_x^{\text{tra}} \\ E_y^{\text{tra}} \end{pmatrix} = \begin{pmatrix} \tau_{xx} & \tau_{xy} \\ \tau_{yx} & \tau_{yy} \end{pmatrix} \begin{pmatrix} E_x^{\text{inc}} \\ E_y^{\text{inc}} \end{pmatrix}. \tag{1}$$

This matrix is analogous to the matrix of reflection coefficients considered in the reflectarray case [23], where τ_{xx} and τ_{yy} are known as the direct coefficients, whose phase control the shape of the copolar component of the radiated field; and τ_{xy} and τ_{yx} are the cross-coefficients.

For the numerical calculation of the transmission matrix in (1), $\overline{T}$ can be expressed as the sum of two matrices, $\overline{T} = \overline{T}_{\text{sub}} + \overline{T}_{\text{met}}$, where $\overline{T}_{\text{sub}}$ accounts for the effects of the substrate in absence of metallizations and $\overline{T}_{\text{met}}$ accounts only for the effect of the metallizations (dipoles in the case of the unit cell shown in Fig. 1). $\overline{T}_{\text{sub}}$ can be readily calculated by means of translation matrices for ungrounded substrates [24].

Matrix $\overline{T}_{\text{met}}$ relates the tangential components of the incident and transmitted fields, in their respective interfaces, that represent only the contributions of the metallizations to the original fields in (1):

$$\begin{pmatrix} E_{x,\text{met}}^{\text{tra}} \\ E_{y,\text{met}}^{\text{tra}} \end{pmatrix} = \begin{pmatrix} \tau_{xx,\text{met}} & \tau_{xy,\text{met}} \\ \tau_{yx,\text{met}} & \tau_{yy,\text{met}} \end{pmatrix} \begin{pmatrix} E_{x,\text{met}}^{\text{inc}} \\ E_{y,\text{met}}^{\text{inc}} \end{pmatrix}. \tag{2}$$

From (2) we can see that when $E_{x,\text{met}}^{\text{inc}} = 1$ and $E_{y,\text{met}}^{\text{inc}} = 0$, then $\tau_{xx,\text{met}} = E_{x,\text{met}}^{\text{tra}}$ and $\tau_{yx,\text{met}} = E_{y,\text{met}}^{\text{tra}}$. On the other hand, when $E_{x,\text{met}}^{\text{inc}} = 0$ and $E_{y,\text{met}}^{\text{inc}} = 1$, then $\tau_{xy,\text{met}} = E_{x,\text{met}}^{\text{tra}}$ and $\tau_{yy,\text{met}} = E_{y,\text{met}}^{\text{tra}}$. Thus, to obtain $\overline{T}_{\text{met}}$ we need to calculate $\vec{E}_{\text{met}}^{\text{tra}}$ for the two incidence cases, which can be obtained, in the absence of grating lobes, as [17]:

$$\begin{aligned} \vec{E}_{\text{met}}^{\text{tra}} = {} & \tilde{\overline{G}}^{c}(k_{x0}, k_{y0}, z = -h, z' = -h) \cdot \tilde{\vec{J}}_1^{d}(k_{x0}, k_{y0}) + \\ & \tilde{\overline{G}}^{c}(k_{x0}, k_{y0}, z = -h, z' = 0) \cdot \tilde{\vec{J}}_2^{d}(k_{x0}, k_{y0}), \end{aligned} \tag{3}$$

where $\tilde{\overline{G}}^{c}$ is a 2×2 matrix of the 2D continuous Fourier transform of the substrate slab non-periodic dyadic Green's function [13]; $\tilde{\vec{J}}_1^{d}$ and $\tilde{\vec{J}}_2^{d}$ are the 2D discrete Fourier transforms of the surface currents induced in the metallizations by an impinging plane wave at the interfaces $z = -h$ and $z = 0$, respectively; $k_{x0} = k_0 \sin\theta_{\text{inc}} \cos\varphi_{\text{inc}}$ and $k_{y0} = k_0 \sin\theta_{\text{inc}} \sin\varphi_{\text{inc}}$ are the transversal wavenumbers of the fundamental Floquet mode; and k_0 is the free-space wavenumber.

Matrix $\tilde{\overline{G}}^{c}$ can be calculated as a particular case of the general algorithm described in [25] when applied to an isotropic ungrounded medium. On the other hand, $\tilde{\vec{J}}^{d}$ is unknown and must be numerically computed by using the MoM in the spectral domain [13]. The MoM is applied to solve an electric field integral equation [16], for which the surface currents in the spatial domain are modelled as a summation of Floquet-periodic entire-domain basis functions:

$$\vec{J}_q(x, y) = \sum_{i=1}^{L} \sum_{p=1}^{2} \sum_{r=1}^{R_p} \sum_{s=1}^{S_p} c_{ip}^{rs}\, \vec{J}_{q,ip}^{rs}(x, y), \tag{4}$$

where c_{ip}^{rs} are the unknown coefficients to be solved by applying MoM, and $\vec{J}_{q,ip}^{rs}(x, y)$, $q = 1, 2$, are known entire-domain basis functions. For the unit cell in Fig. 1, the number of metallizations is $L = 5$ per interface, subindex p indicates the component of $\vec{J}$ ($\hat{x}$ or $\hat{y}$), and $N = R_1 S_1 + R_2 S_2$ is the total number of basis functions per metallization.

The entire domain basis functions employed in (4) are based on Chebyshev polynomials weighed by a function that accounts for edge singularities at the metallizations border [16], [26] that take the form:

$$\vec{J}_{q,i1}^{rs}(x, y) = \frac{-jk_0}{2rw} U_{r-1}(C_{x,q,i}) \sqrt{1 - C_{x,q,i}^2}\, \frac{T_{s-1}(C_{y,q,i})}{\sqrt{1 - C_{y,q,i}^2}}\, \hat{x}, \tag{5a}$$

$$(q = 1, 2;\ i = 1, \ldots, L;\ r = 1, \ldots, R_1;\ s = 1, \ldots, S_1),$$

$$\vec{J}_{q,i2}^{rs}(x, y) = \frac{-jk_0}{2sl_i} \frac{T_{r-1}(C_{x,q,i})}{\sqrt{1 - C_{x,q,i}^2}} U_{s-1}(C_{y,q,i}) \sqrt{1 - C_{y,q,i}^2}\, \hat{y}, \tag{5b}$$

$$(q = 1, 2;\ i = 1, \ldots, L;\ r = 1, \ldots, R_2;\ s = 1, \ldots, S_2),$$

where T_{n-1} and U_{n-1} are the degree $(n-1)$ Chebyshev polinomials or first and second kind, respectively, and:

$$C_{x,q,i} = 2\left(x - x_{c,q,i}\right)/l_i \,, \tag{6a}$$

$$C_{y,q,i} = 2\left(y - y_{c,q,i}\right)/w \,. \tag{6b}$$

The MoM in the spectral domain as well as (3) require the knowledge of the Fourier transform of the basis functions in (5), which are:

$$\tilde{\vec{J}}^{d,rs}_{q,i1}(k_{xm}, k_{yn}) = \frac{k_0\pi^2}{4k_{xm}p_x p_y}(-j)^{r+s-1} B_r\left(\frac{k_{xm}l_i}{2}\right) \cdot B_{s-1}\left(\frac{k_{yn}w}{2}\right) e^{-j\left(k_{xm}x_{c,q,i}+k_{yn}y_{c,q,i}\right)}\hat{x}, \tag{7a}$$

$$\tilde{\vec{J}}^{d,rs}_{q,i2}(k_{xm}, k_{yn}) = \frac{k_0\pi^2}{4k_{yn}p_x p_y}(-j)^{r+s-1} B_{r-1}\left(\frac{k_{xm}l_i}{2}\right) \cdot B_{s}\left(\frac{k_{yn}w}{2}\right) e^{-j\left(k_{xm}x_{c,q,i}+k_{yn}y_{c,q,i}\right)}\hat{y}, \tag{7b}$$

where B_k is the Bessel function[1] of first kind and order k, and the spectral variables $k_{xm} = k_{x0} + 2\pi m/p_x$ and $k_{yn} = k_{y0} + 2\pi n/p_y$. It is worth noting that there is a singularity in (7) when $k_{xm} = 0$ or $k_{yn} = 0$. This can be circumvented in those cases by employing the asymptotic expansion of the Bessel function for small arguments [27, eq. (9.1.7)].

Finally, we can express the surface current of (4) in the spectral domain as a linear combination of (7) thanks to the linearity of the Fourier transform:

$$\tilde{\vec{J}}^{d}_{q}(k_{xm}, k_{yn}) = \sum_{i=1}^{L}\sum_{p=1}^{2}\sum_{r=1}^{R_p}\sum_{s=1}^{S_p} c^{rs}_{ip}\,\tilde{\vec{J}}^{d,rs}_{q,ip}(k_{xm}, k_{yn}), \tag{8}$$

which allows to compute (3) after solving for the c^{rs}_{ip} coefficients with MoM.

C. Comparison with Circuit Model

In order to validate the proposed analysis technique for TA unit cells we will compare MoM simulations of the structure shown in Fig. 1 with simulations based on a circuit model from [18, Fig. 7], Ansys HFSS [28] and CST [29]. Fig. 2 shows the electromagnetic response of the unit cell in magnitude and phase in the E-band. The MoM results present closer agreement with HFSS and CST than the circuit model, which would generally only work for the frequency range for which it was optimized. In addition, the MoM is considerably faster than HFSS and CST. In fact, the MoM took 0.9 s to simulate the 51 points in Fig. 2, in a laptop with an AMD Ryzen 7 7840u CPU, using around 6 MB of memory. On the other hand, HFSS took around 50 min and 3 GB of memory to complete the same points, while for CST took 55 min and 7.6 GB. Thus, the MoM is three orders of magnitude faster than HFSS and CST while employing two orders of magnitude less memory.

[1]We use B instead of the usual J to denote the Bessel function to avoid confusion with the surface currents notation.

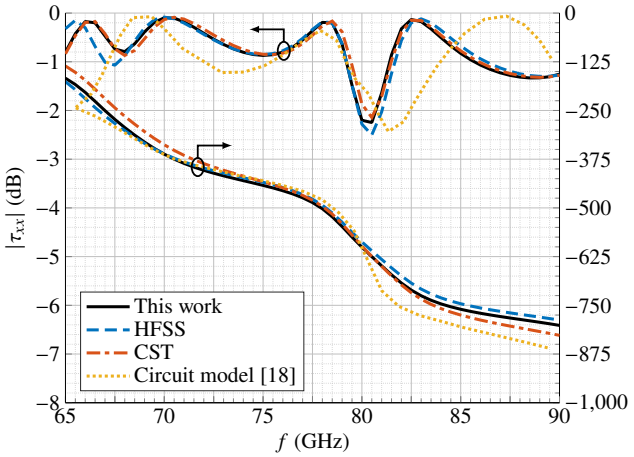

Fig. 2. Comparison of the proposed technique with HFSS and CST simulations as well as the circuit model from [18, Fig. 7] for normal incidence. The unit cell geometrical parameters are: $p_x = p_y = 2.401$ mm, $h = 0.508$ mm, $\varepsilon_r = 2.2$, $\tan\delta = 0.0009$, $w = 0.075$ mm, $l_{1,1} = l_{1,5} = l_{2,1} = l_{2,5} = 1.138$ mm, $l_{1,2} = l_{1,4} = l_{2,2} = l_{2,4} = 1.366$ mm, $l_{1,3} = l_{2,3} = 1.655$ mm, $x_{c,1,1} = x_{c,1,5} = 1.408$ mm, $x_{c,1,2} = x_{c,1,4} = 1.4495$ mm, $x_{c,1,3} = 1.4915$ mm, $y_{c,1,1} = 0.8745$ mm, $y_{c,1,2} = 1.0375$ mm, $y_{c,1,3} = 1.2005$ mm, $y_{c,1,4} = 1.3635$ mm, $y_{c,1,5} = 1.5265$ mm. Centre coordinates of metallizations in the top layer can be obtained by rotating 180° the metallizations of the bottom layer. The number of basis functions per metallization employed here was seven ($R_1 = 5$, $S_1 = 1$, $R_2 = 1$, $S_2 = 2$).

III. Unit Cell for W-band Transmitarray Design

A. Practical Unit Cell Parameters

Although the developed analysis technique based on the MoM is general regarding the position of the dipoles, for practical designs specifying the central coordinates of each dipole is cumbersome. To facilitate the design of the unit cell, we will employ a slightly variation of the unit cell of [18] with some simplifications on the parameters. First, the centre coordinates of the dipoles in each interface are aligned, that is, the coordinate $x_{c,1,i}$ and $x_{c,2,i}$ will be the same for $i = 1, \ldots, 5$, but $x_{c,1,i} \neq x_{c,2,i}, \forall i$. We will also define the length of lateral dipoles with a scaling factor $\alpha_{q,i} \in (0, 1)$ with regard to the length of the central dipole of the bottom interface, which will be one of the design parameters:

$$l_{q,i} = \alpha_{q,i} l_{1,3}; \quad q = 1, 2; \quad i = 1, \ldots, 5. \tag{9}$$

The second design parameter is the overlap Δ between central dipoles ($i = 3$) of both interfaces. In addition, it is worth introducing one more parameter, the distance between dipoles g (see Fig. 1).

With these parameters, the $y_{c,q,i}$ coordinate can be obtained from g and the width w of the dipoles, while coordinate $x_{c,q,i}$ can be obtained from the two design parameters Δ and $l_{1,3}$ as:

$$x_{c,1,i} = (p_x - \Delta + l_{1,3})/2, \quad i = 1, \ldots, 5 \tag{10a}$$

$$x_{c,2,i} = (p_x + \Delta - l_{1,3})/2, \quad i = 1, \ldots, 5 \tag{10b}$$

As reference, $g = 0.088$ mm, $\Delta = 1.073$ mm, $\alpha_{1,1} = \alpha_{2,1} = \alpha_{1,5} = \alpha_{2,5} = 0.688$, $\alpha_{1,2} = \alpha_{2,2} = \alpha_{1,4} = \alpha_{2,4} = 0.825$, $\alpha_{1,3} = \alpha_{2,3} = 1$ for the cell simulated in Fig. 2. Finally, for practical TA design, the unit cell needs to provide enough phase-shift at a single frequency. This is achieved by scaling the design

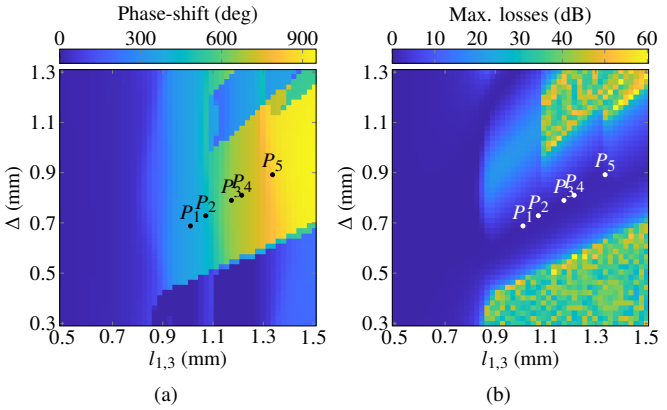

Fig. 3. Parametric sweep in Δ and $l_{1,3}$ showing (a) the maximum phase-shift range and (b) maximum losses for $\beta \in [0.6, 1.15]$ at 105 GHz. The values for the five points are shown in Table I.

parameters Δ and $l_{1,3}$ by a factor $\beta > 0$ and sweeping that factor. The only restriction is that $\beta\, l_{1,3} < p_x$.

B. Unit Cell Design at W-band

With the proposed analysis method, the goal is to design a TA unit cell that works in W-band in the range 102 GHz–109.5 GHz as proposed by the ITU [3]. As a first approximation to obtain some of the parameters, we will apply a scaling factor of 0.733, which is the ratio between the central frequencies of the range shown in Fig. 2 and the range in the W-band proposed by the ITU. This gives a periodicity $p_x = p_y = 1.76$ mm, length of central dipoles $l_{1,3} = l_{2,3} = 1.213$ mm, an overlap $\Delta = 0.787$ mm, separation between dipoles $g = 0.065$ mm and dipole width of $w = 0.055$ mm. The scaling factors $\alpha_{q,i}$ will be the same as in Fig. 2. If the substrate thickness is also scaled by the same factor of 0.733, obtaining a thickness $h = 0.372$ mm, the performance of the unit cell is very good, achieving a maximum phase-shift range of more than 600° and maximum transmission losses of 1.6 dB for $\beta \in [0.6, 1.15]$ at 105 GHz. However, a substrate thickness of $h = 0.372$ mm is not commercially available and when using available thicknesses, performance quickly deteriorates. For instance, with a thickness of $h = 0.508$ mm the maximum transmission losses increase to more than 3.6 dB.

Thus, the goal is to find appropriate values of Δ and $l_{1,3}$ such that when they are scaled by $\beta \in [0.6, 1.15]$ the phase range is large while minimizing the maximum transmission losses in the same range of β. Doing such optimization or parametric analysis in HFSS would be very time consuming. However, with the proposed analysis technique, it is relatively fast. A parametric sweep in the plane $\Delta \times l_{1,3}$, with $\Delta \in [0.3, 1.2]$ mm, $l_{1,3} \in [0.5, 1.5]$, with 50 points for Δ and $l_{1,3}$, and 80 points for β (200 000 calls to the MoM routine) took around one hour to complete at 105 GHz and quickly found optimal results with low transmission losses and very large phase-shift range.

Fig. 3 shows the results of the parametric sweep in the $\Delta \times l_{1,3}$ plane. There is a narrow path where there are low maximum losses and large phase-shift. Specific values for five points are shown in Table I. They provide losses lower than 2 dB and enough phase-shift to carry out TA design and optimization. Point P_4 was selected as a trade-off between maximum losses and large phase-range to carry out an in-band simulation to analyse the performance at extreme frequencies within the band of interest. Results of this simulation are shown in Fig. 4, comparing MoM and HFSS. The phase-shift range is still large at other frequencies and losses are relatively low, although slightly larger than at central frequency. Maximum losses are −1.3 dB and −1.6 dB at 100 GHz and 110 GHz, respectively, while the maximum phase-shift range is 617 deg and 733 deg. Similar results are obtained in terms of efficiency and accuracy for oblique incidence.

This technique can thus be used for practical transmitarray layout design taking into account the real angle of incidence [30], wideband [31] or shaped-beam [32], [33] optimization or sample generation for machine learning training [23], all within an acceptable computing time.

Table I
VALUES OF THE FIGURES-OF-MERIT FOR THE POINTS SHOWN IN FIG. 3, CALCULATED FOR $\beta \in [0.6, 1.15]$ AT 105 GHZ.

Point	Δ (mm)	$l_{1,3}$ (mm)	Phase range (deg)	Max. losses (dB)	Avg. losses (dB)
P_1	1.010	0.688	358	1.027	0.738
P_2	1.071	0.729	429	1.076	0.756
P_3	1.173	0.790	657	1.106	0.703
P_4	1.214	0.810	689	1.132	0.696
P_5	1.337	0.892	846	1.742	0.767

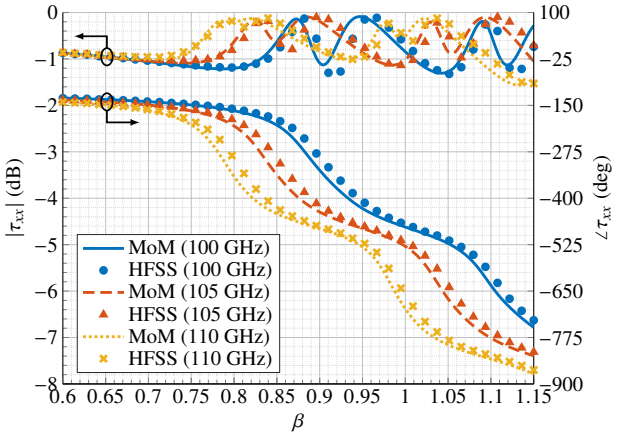

Fig. 4. In band simulation of the optimized unit cell comparing MoM and HFSS simulations for point P_4 from Fig. 3 and Table I. The number of basis functions per dipole was seven ($R_1 = 5$, $S_1 = 1$, $R_2 = 1$, $S_2 = 2$).

IV. Conclusion

A technique based on the method of moments (MoM) in the spectral domain has been developed for the efficient analysis of transmitarray unit cells based on rectangular metallizations. It was applied to the analysis and optimization of a highly resonant Huygens' element at E- and W-bands. Comparison with circuit models show that the proposed technique offers more accurate results while being up to three orders of magnitude faster than full-wave simulations with general purpose commercial software, as well as using far less memory resources.

REFERENCES

[1] W. Hong, Z. H. Jiang, C. Yu, D. Hou, H. Wang, C. Guo, Y. Hu, L. Kuai, Y. Yu, Z. Jiang, Z. Chen, J. Chen, Z. Yu, J. Zhai, N. Zhang, L. Tian, F. Wu, G. Yang, Z.-C. Hao, and J. Y. Zhou, "The role of millimeter-wave technologies in 5G/6G wireless communications," *IEEE J. Microw.*, vol. 1, no. 1, pp. 101–122, 2021.

[2] S. Islam, Z. A. Atallah, A. K. Budati, M. K. Hasan, R. Kolandaisamy, and S. Nurhizam, "Mobile networks toward 5G/6G: Network architecture, opportunities and challenges in smart city," *IEEE Open J. Commun. Soc.*, 2024, early access.

[3] International Telecommunication Union – Radiocommunication Sector, Ed., *World Radiocommunication Conference: Final Acts*, 20 Nov–12 Dec 2023.

[4] C. Paoloni, "Sub-THz wireless transport layer for ubiquitous high data rate," *IEEE Commun. Mag.*, vol. 59, no. 5, pp. 102–107, 2021.

[5] P. Heydari, "Terahertz integrated circuits and systems for high-speed wireless communications: Challenges and design perspectives," *IEEE Open J. Solid-State Circuits Soc.*, vol. 1, pp. 18–36, 2021.

[6] N. Moraitis and K. S. Nikita, "Ray-tracing propagation modeling in urban environment at 140 GHz for 6G wireless networks," *IEEE Access*, vol. 11, pp. 133 835–133 849, 2023.

[7] International Telecommunication Union – Radiocommunication Sector, "Technical feasibility of IMT in bands above 100 GHz," ITU, Geneva, France, Tech. Rep., May 2024.

[8] A. H. Abdelrahman, F. Yang, A. Z. Elsherbeni, and P. Nayeri, *Analysis and Design of Transmitarray Antennas*. San Rafael, CA, USA: Morgan & Claypool, 2017.

[9] S. L. Liu, X. Q. Lin, Z. Q. Yang, Y. J. Chen, and J. W. Yu, "W-band low-profile transmitarray antenna using different types of FSS units," *IEEE Trans. Antennas Propag.*, vol. 66, no. 9, pp. 4613–4619, 2018.

[10] S. Shi, Q. Lu, W. Feng, and W. Chen, "Wideband polarization rotation transmitarray using arrow-shaped FSS at W-band," *IEEE Trans. Antennas Propag.*, vol. 70, no. 7, pp. 6001–6005, 2022.

[11] K. K. K. Ho, G.-B. Wu, B.-J. Chen, K. F. Chan, and C. H. Chan, "Spot focusing coma correction by linearly polarized dual-transmitarray antenna in the terahertz region," *IEEE Trans. THz Sci. Technol.*, vol. 13, no. 5, pp. 493–502, 2023.

[12] X. He, W. Yang, Y. Li, Q. Xue, and W. Che, "W-band wideband transmit-array antenna based on multiresonance multimode Huygens metasurface," *IEEE Trans. Antennas Propag.*, vol. 72, no. 9, pp. 7299–7304, 2024.

[13] R. Mittra, C. H. Chan, and T. Cwik, "Techniques for analyzing frequency selective surfaces—a review," *Proc. IEEE*, vol. 76, no. 12, pp. 1593–1615, 1988.

[14] D. M. Pozar, S. D. Targonski, and H. D. Syrigos, "Design of millimeter wave microstrip reflectarrays," *IEEE Trans. Antennas Propag.*, vol. 45, no. 2, pp. 287–296, Feb. 1997.

[15] J. A. Encinar, "Design of two-layer printed reflectarrays using patches of variable size," *IEEE Trans. Antennas Propag.*, vol. 49, no. 10, pp. 1403–1410, Oct. 2001.

[16] R. Florencio, R. R. Boix, E. Carrasco, J. A. Encinar, and V. Losada, "Efficient numerical tool for the analysis and design of reflectarrays based on cells with three parallel dipoles," *Microw. Opt. Technol. Lett.*, vol. 55, no. 6, pp. 1212–1216, Jun. 2013.

[17] R. F. Díaz, "Contribución al análisis eficiente y a la mejora de prestaciones de antenas reflectarray," Ph.D. dissertation, Universidad Politécnica de Madrid, 2015, (in spanish).

[18] X. Wang, P.-Y. Qin, L.-Z. Song, R. Jin, and Y. J. Guo, "Tightly coupled Huygens element-based conformal transmitarray for E-band airborne communication systems," *IEEE Trans. Antennas Propag.*, vol. 71, no. 3, pp. 2467–2475, 2023.

[19] Z. H. Jiang, F. Wu, T. Yue, and W. Hong, "Wideband and low-profile integrated dual-circularly-polarized transmit-arrays enabled by antenna-filter-antenna phase shifting cells," *IEEE Trans. Antennas Propag.*, vol. 69, no. 11, pp. 7462–7475, 2021.

[20] W. Yang, K. Chen, J. Zhao, T. Jiang, and Y. Feng, "Frequency-multiplexed spin-decoupled metasurface for low-profile dual-band dual-circularly polarized transmitarray with independent beams," *IEEE Trans. Antennas Propag.*, vol. 72, no. 1, pp. 642–652, 2024.

[21] C. Pfeiffer and A. Grbic, "Metamaterial Huygens' surfaces: Tailoring wave fronts with reflectionless sheets," *Phys. Rev. Lett.*, vol. 110, pp. 197 401 (1–5), May 2013.

[22] A. Epstein and G. V. Eleftheriades, "Huygens' metasurfaces via the equivalence principle: design and applications," *J. Opt. Soc. Am. B*, vol. 33, no. 2, pp. A31–A50, Feb. 2016.

[23] D. R. Prado, P. Naseri, J. A. López-Fernández, S. V. Hum, and M. Arrebola, "Support vector regression-enabled optimization strategy of dual circularly-polarized shaped-beam reflectarray with improved cross-polarization performance," *IEEE Trans. Antennas Propag.*, vol. 71, no. 1, pp. 497–507, 2023.

[24] J. L. Tsalamengas, "Interaction of electromagnetic waves with general bianisotropic slabs," *IEEE Trans. Microw. Theory Techn.*, vol. 40, no. 10, pp. 1870–1878, 1992.

[25] F. L. Mesa, R. Marques, and M. Horno, "A general algorithm for computing the bidimensional spectral green's dyad in multilayered complex bianisotropic media: the equivalent boundary method," *IEEE Trans. Microw. Theory Techn.*, vol. 39, no. 9, pp. 1640–1649, 1991.

[26] W. C. Chew and Q. Liu, "Resonance frequency of a rectangular microstrip patch," *IEEE Trans. Antennas Propag.*, vol. 36, no. 8, pp. 1045–1056, 1988.

[27] M. Abramowitz and I. A. Stegun, Eds., *Handbook of Mathematical Functions with Formulas, Graphs, and Mathematical Tables*. Washington, D.C., USA: United States Department of Commerce, National Bureau of Standards (NBS), 1972, tenth printing.

[28] "HFSS," Ansys Inc., Pittsburgh, Pennsylvania, USA.

[29] "CST," Dassault Systèmes SE, Vélizy-Villacoublay, France.

[30] E. R. F. Almajali and D. A. McNamara, "Angle of incidence effects in reflectarray antenna design: Making gain increases possible by including incidence angle effects," *IEEE Antennas Propag. Mag.*, vol. 58, no. 5, pp. 52–64, 2016.

[31] R. Florencio, J. A. Encinar, R. R. Boix, V. Losada, and G. Toso, "Reflectarray antennas for dual polarization and broadband telecom satellite applications," *IEEE Trans. Antennas Propag.*, vol. 63, no. 4, pp. 1234–1246, Apr. 2015.

[32] D. R. Prado, M. Arrebola, M. R. Pino, R. Florencio, R. R. Boix, J. A. Encinar, and F. Las-Heras, "Efficient crosspolar optimization of shaped-beam dual-polarized reflectarrays using full-wave analysis for the antenna element characterization," *IEEE Trans. Antennas Propag.*, vol. 65, no. 2, pp. 623–635, Feb. 2017.

[33] M. Zhou, S. B. Sørensen, O. S. Kim, E. Jørgensen, P. Meincke, and O. Breinbjerg, "Direct optimization of printed reflectarrays for contoured beam satellite antenna applications," *IEEE Trans. Antennas Propag.*, vol. 61, no. 4, pp. 1995–2004, Apr. 2013.